

## *f*-band dispersion in UIr<sub>3</sub>: An angle-resolved and resonant photoemission study

A. J. Arko and D. D. Koelling

*Argonne National Laboratory, Argonne, Illinois 60439*

B. Reihl

*IBM Zurich Research Laboratory, CH-8803 Rüschlikon, Switzerland*

(Received 7 September 1982)

Angle-resolved photoemission measurements using synchrotron radiation have been made on a UIr<sub>3</sub>(100) face. With the use of the Fano resonance at the 5*d* absorption edge, the 5*f* emission was extracted and found to agree well with a calculated 5*f* density of states. Dispersion was observed for the first time in a photoemission peak clearly associated with 5*f* emission. The dispersion is generally in good agreement with calculated energy bands.

### I. INTRODUCTION

Actinide metals and intermetallic compounds display complex electronic, magnetic, structural, and superconducting properties.<sup>1</sup> While 6*d* electrons clearly play a role,<sup>2,3</sup> it is generally believed that 5*f* electrons in possibly hybridized energy bands are particularly important.<sup>4</sup> Obviously, an understanding of the electronic band structure, and hence the role of the 5*f* electrons, is an important element in any explanation of actinide properties. Of particular interest is the question of localization versus itinerancy of 5*f* electrons, and their participation in bonding in compounds.

Recently, it has been shown that a Fano-type resonance<sup>5</sup> is observed in the photoemission spectra of actinide materials<sup>6-8</sup> as the photon energy is tuned through the 5*d*-core absorption edge. Characteristic *f*-electron features can be identified in photoemission spectra and extracted by using these resonant photoemission techniques. From such measurements one cannot of course determine *a priori* the localized versus itinerant nature of 5*f* electrons, but one can unambiguously determine the energy position of the 5*f* features. Moreover, it is often possible to deduce the extent of hybridization with *p* or *d* electrons.<sup>8,9</sup>

Previous resonant photoemission studies<sup>6-8</sup> in uranium compounds have only considered clearly localized or "quasilocalized" cases, since resonant photoemission is well understood in the atomic case. Of particular importance was the study<sup>8</sup> on UO<sub>2</sub>, which has a localized 5*f* level well separated from the valence bands. It was found that at the antiresonance (92 eV) the 5*f* emission becomes almost vanishingly small. This allows an accurate extraction of 5*f* features.

In this paper we present results of a resonant photoemission study (using tunable synchrotron ra-

diation) of UIr<sub>3</sub>, a compound where from previous measurements<sup>10-14</sup> it is known that the 5*f* electrons are purely itinerant. This material is of particular importance because it is one of the few actinide materials for which a complete set of band-structure calculations is corroborated by de Haas-van Alphen (dHvA) data.<sup>12,13</sup> We have now performed self-consistent calculations for UIr<sub>3</sub>, and we use those results in this paper. Orbital decomposition of the wave functions was performed, so that it is possible in this material to compare directly the *f*-electron portion of the photoemission spectrum with a calculated partial density of *f* states. This should give us a good indication of the reliability of such procedures in materials where no calculations exist.

In Sec. II, we give the experimental details while in Sec. III we present the theoretical background on the self-consistent calculation. The experimental results are discussed in terms of these calculations in Sec. IV; in particular, the total and partial density of states is discussed as well as the first experimental observation of 5*f*-band dispersion.

### II. EXPERIMENTAL

A <100>-oriented single-crystal sheet of UIr<sub>3</sub> (grown by electron-beam zone melting<sup>10</sup>) was used in the present study. The (100) surface was prepared by 600-eV Ne-ion bombardment and simultaneous annealing at  $\approx 600^\circ\text{C}$  for 2 h. Flashing to  $\sim 800^\circ\text{C}$  completed the cleaning cycle. The surface conditions were monitored using Auger spectroscopy and low-energy electron diffraction (LEED). In addition, any buildup of oxygen or CO on the surface was observed as additional photoemission peaks in the (6-14)-eV binding-energy range. LEED revealed the reconstructed  $c(2\times 8)$  surface in agreement with earlier findings.<sup>15</sup> After the initial clean-

ing and annealing, subsequent buildup of CO and O could be removed by simply flashing to  $\sim 800^\circ\text{C}$  for a few seconds.

The photoemission measurements were performed with a two-dimensional display-type analyzer<sup>16</sup> using synchrotron radiation in the range  $10\text{ eV} \leq h\nu \leq 130\text{ eV}$ , at the Synchrotron Radiation Center of the University of Wisconsin—Madison. The system can be operated both in the angle-integrated ( $\Delta\theta=86^\circ$ ) and angle-resolved ( $\Delta\theta=6^\circ$ ) modes with an energy resolution of 0.15 eV.

### III. THEORETICAL CONSIDERATIONS

The band structure utilized in this paper was calculated using a linearized variant of the relativistic augmented-plane-wave method. Thus all relativistic kinematic effects including spin-orbit coupling have been included. The potential was included in the warped—muffin-tin approximation<sup>17</sup> where it is spherically averaged inside the muffin-tin spheres, but no approximation was made in the interstitial region. The potential is the result of performing a self-consistent calculation utilizing only exchange as the exchange-correlation functional. During the self-consistency cycles, only the so-called scalar relativistic effects were included while spin-orbit coupling was omitted. The effects of using a different exchange-correlation functional cannot be resolved in this experiment so we will not discuss them here. Some discussion regarding the omitting of the spin-orbit coupling during the self-consistent-field (SCF) cycles is appropriate, however. This is a weak point of the calculation, a result of purely economic considerations. In many cases it is a very good approximation, since the spin-orbit coupling has very little effect on the shape of the charge density. Moreover, the reader is reminded that spin orbit is included in the calculation once the potential is determined. The major effect to be expected is through its influence on the selection of occupied states. In the case of  $\text{UIr}_3$ , both the U  $f$  and Ir  $d$  have large spin-orbit couplings. Since the levels at  $\Gamma$  are considerably changed near the Fermi energy due to spin-orbit coupling, the occupation of states in this area is strongly affected. Hence neglect of spin-orbit coupling causes more states of U  $f$  character to be occupied in the vicinity of  $\Gamma$ . It is difficult to ascertain what states are thereby omitted with the inclusion of spin-orbit as they are not uniform in all regions of space. One expects them to have less  $f$  character, however. The omission of spin-orbit coupling during the SCF cycles then probably results in a potential reflecting slightly too much  $f$  character. This would place the states with  $f$ -orbital content slightly too high.

A prior non-self-consistent calculation<sup>13,14,18</sup> has been used to interpret de Haas—van Alphen data available for  $\text{UIr}_3$ . That calculation had adjusted the atomic configurations used in an overlapping charge-density (OCD) model. The best potential was obtained using  $\text{U}(f^3d^2s^1)$  and  $\text{Ir}(d^9)$ . In the present calculation, the analysis of the charge inside the muffin-tin spheres yields  $\text{U}(f,2.41; d,1.22; s, 0.20; p,0.30)$  and  $\text{Ir}(d,6.73 s,0.61; p,0.50)$ . These cannot be taken as atomic configurations as the  $s$ ,  $p$ , and  $d$  orbitals extend considerably beyond the muffin-tin spheres. At the level that OCD configurations are significant to our deliberations, one might have preferred to have an  $\text{Ir}(d^8s^1)$  configuration for the earlier calculation. We make contact with that earlier calculation because it experienced some success in interpreting the major piece of the Fermi surface, a large open surface centered at the point  $M$ . That surface is found as well in the more recent SCF calculation. Moreover, a small neck along the  $\langle 100 \rangle$  directions (i.e., through  $R$ ) is found in this calculation. Such a neck was postulated to exist, based on dHvA data, but was not found in the previous calculation. A large neck along the  $\Gamma M$  direction is found in both calculations.

The structure at  $\Gamma$  is considerably different between the two calculations and is also sensitive to the presence of spin-orbit coupling. A qualitative examination indicates the existence in the present calculation of two closed  $d$ -band surfaces at  $\Gamma$ , which are needed to explain dHvA data. Likewise, a larger  $f$ -like surface is found at  $R$ , all consistent with dHvA data and not found in the previous calculation. While a detailed comparison between the SCF calculation and dHvA data will be the subject of a future paper, suffice it to say that the band structure presented here is in better qualitative agreement with dHvA data than the earlier results, where the agreement with the large surface at  $M$  was already quite good.

### IV. RESULTS AND DISCUSSION

#### A. Density of states and EDC's

The dashed curve of Fig. 1(a) represents an angle-integrated energy distribution curve (EDC) obtained at resonance ( $h\nu=98\text{ eV}$ ) where  $f$ -electron features are resonantly enhanced. In general, very little difference was noted between the angle-integrated and angle-resolved spectra above  $\approx 40\text{ eV}$ . Five distinct features are observed [labeled  $A$  through  $E$  in Fig. 1(a)] similar to the related compound  $\text{UPd}_3$ .<sup>8,19</sup> We can compare the curve of Fig. 1(a) to the calculated total density of states (DOS) shown in Fig. 1(b) which was obtained from the cal-

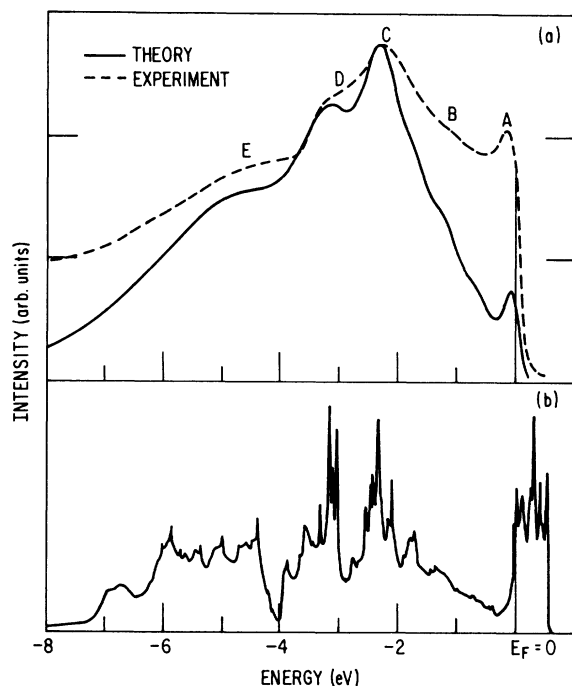


FIG. 1. (a) Electron distribution curve (dashed line) obtained from UIr<sub>3</sub>(100) at a photon energy of 98 eV, superimposed on a calculated total density of states for UIr<sub>3</sub> (solid line) which has been broadened by both an instrument and a lifetime broadening function. (b) The unbroadened density of states.

calculations described in the preceding section. The total DOS of Fig. 1(b) was Gaussian-broadened first by an instrument broadening function using 0.15 eV as full width at half maximum (FWHM) and then also by an energy-dependent lifetime broadening function where the FWHM was assumed to be of the form<sup>20</sup>  $\alpha(E-E_F)^2$  (best fit  $\alpha \approx 0.05$ ). The resulting broadened DOS is shown as the solid curve of Fig. 1(a) which has been normalized to the experimental curve at peak C. Except for the amplitude discrepancy for features A and B (primarily due to the *5f* resonance enhancement at  $h\nu=98$  eV) we can claim quite good agreement. From a decomposition of the total theoretical DOS into partial DOS's we learn that feature C corresponds to Ir *d*<sub>5/2</sub> emission, while D is primarily Ir *d*<sub>3/2</sub>. The occupied portion of the *f*-electron bands is  $\sim 3$  eV wide and strongly hybridized with the *d* bands. It is *d*-electron photoemission which constitutes the bulk of the emission features. Indeed, a similarly broadened partial DOS for *d* bands only (no *f* contribution) results in a curve almost indistinguishable from the solid curve of Fig. 1(a) except for peak A which is primarily *f*-like in character.

### B. *f*-electron DOS

Figure 2 shows photoemission spectra taken at resonance (98 eV) and at the antiresonance (92 eV). If we assume that in the antiresonance all *f*-electron emission is suppressed<sup>8</sup> as in the case of UO<sub>2</sub>, and that the Ir *d* emission is unchanged, then a subtraction of the two curves (after normalizing at the point shown by the arrow) yields the *f* spectrum (dotted curve of Fig. 2) which should be representative of the *f*-electron DOS. This confirms that peak A is primarily "*f*-like" while the remaining *f* density is hybridized and distributed in the *d* bands.

In Fig. 3 we compare this difference curve to a calculated partial *f* DOS, where the calculated DOS was convoluted with the same broadening functions used for the total DOS of Fig. 1(a). The curves were normalized at peak A. While the agreement is less satisfying than in Fig. 1 for the total DOS, it is certainly encouraging. There is agreement on the bandwidth and binding energies of the peaks, while there is disagreement on the relative amplitudes. Part of this problem was somewhat anticipated. We did not remove the secondaries<sup>9</sup> from our spectra nor did we take any change in the Ir *d* emission into account.<sup>21</sup> Moreover, the uranium *6d*-electron resonance,<sup>8</sup> expected to be smaller than *5f* resonance by an order of magnitude, likewise was not taken into account. Further, the comparison is only to a broadened DOS

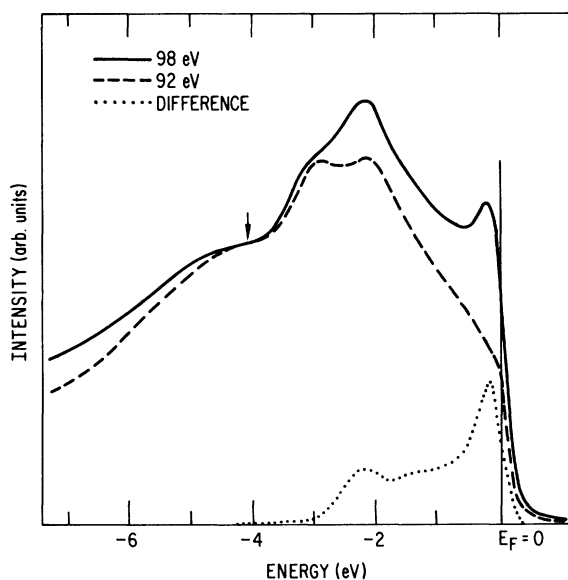


FIG. 2. Photoemission spectra for UIr<sub>3</sub>(100) at resonance (solid line, 98 eV) and at the antiresonance (dashed line, 92 eV). The dotted curve is a subtraction of the two spectra and should represent only the *f*-electron contribution to the photocurrent.

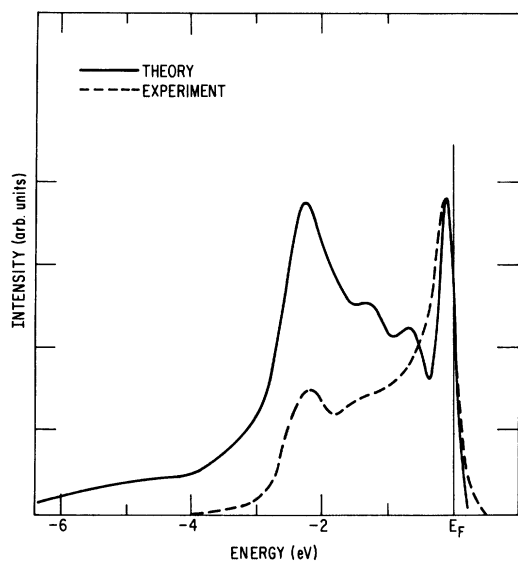


FIG. 3. Comparison of the experimentally extracted  $f$ -electron features in the photocurrent (dashed line) to the calculated  $f$  density of states (solid line) broadened by the same broadening functions as in Fig. 1.

with no consideration of transition probabilities. With this in mind then, we believe that the agreement is quite good. This result, in fact, leads us to believe that in general a partial  $5f$  DOS can be extracted from photoemission spectra using tunable photons at the  $5d$  absorption edge.

A spectrum such as that obtained in Fig. 3 can probably be interpreted in terms of itinerant or band states even without the aid of a band-structure calculation. To begin with, the 3-eV-wide spectrum is pinned to  $E_F$ , a necessary although not a sufficient condition for itineracy.<sup>19</sup> Then too, the observed features in the  $f$  spectrum do not correspond to any of the known multiplet structures<sup>22</sup> found in actinides. Adding to the circumstantial evidence is the dispersion observed for peak  $A$  (discussed in the following section).

### C. Band dispersion

Angle-resolved photoemission EDC's from the  $\text{UIr}_3(100)\text{-}c(2 \times 8)$  surface where obtained both at constant polar angle ( $\theta=0^\circ$ , normal emission), while varying the photon energy, and a constant photon energy ( $h\nu=26$  eV), while varying the polar angle. Figure 4 shows the simple cubic Brillouin zone for the  $\text{UIr}_3$  lattice ( $\text{AuCu}_3$  type). At normal emission for a  $(100)$  surface we are probing the filled states along the  $\Gamma$ - $X$  direction. The angular variation was performed in the  $\langle 100 \rangle$  azimuth so that we are probing states having  $\vec{k}_{\parallel}$  (electron momentum paral-

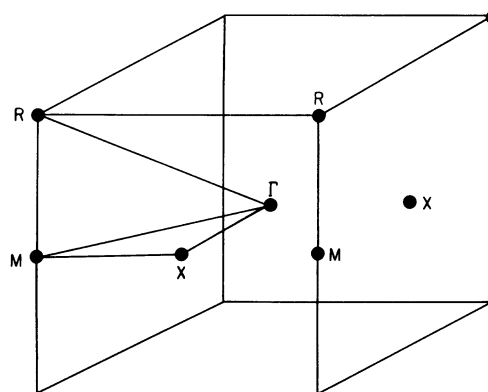


FIG. 4. Brillouin zone for the simple cubic lattice (obtained for a  $\text{Cu}_3\text{Au}$ -type lattice).

lel to the sample surface) parallel to (but not necessarily on) the  $X$ - $M$  line in the  $\Gamma$ - $M$ - $X$  plane.

Normal-emission EDC's versus  $16 \text{ eV} \leq h\nu \leq 40 \text{ eV}$  are shown in Fig. 5. We note several spectral features (denoted  $a$ - $h$ ), some of which show little, but nonetheless significant change in their energetic positions with  $h\nu$ . For  $h\nu \geq 40 \text{ eV}$  no band dispersion is observed and angle-resolved and angle-integrated EDC's are nearly identical. In addition to the usual  $k$  broadening due to the short mean free path of photoelectrons<sup>23</sup> [which destroys all  $E(\vec{k})$  information at higher  $h\nu$  for high- $Z$  heavy materials], we believe that broadening is also occurring as a result of surface umklapp processes due to additional scattering from  $c(2 \times 8)$  surface reciprocal-lattice vectors, as was observed for the  $\text{Ir}(100)\text{-}(5 \times 1)$  surface.<sup>24</sup> The gradual increase (with  $h\nu$ ) in  $\vec{k}$  smearing is clearly demonstrated by feature  $e$ , which shows a gradual increase in amplitude with  $h\nu$  and is nondispersive above  $h\nu \approx 23 \text{ eV}$ . The calculated band structure (see Fig. 6) predicts no band states at  $-4.5 \text{ eV}$  along the  $\Gamma$ - $X$  line (except very near  $X$ ), while several flat Ir-derived  $d$  bands are obtained along the  $X$ - $M$  line yielding peak  $E$  in angle-integrated data [Fig. 1(a)]. Thus feature  $e$  in Fig. 5 can only be observed in normal emission as a result of significant  $k$  broadening, although near the  $X$  point feature  $e$  is probably a legitimate angle-resolved band state. With this in mind then, we have restricted ourselves to  $h\nu < 30 \text{ eV}$  in analyzing normal-emission data, realizing that some residual  $k$  smearing exists even in this range. Feature  $g$  is due to surface impurities and was readily eliminated by flashing the sample to  $600^\circ\text{C}$ .

Peak  $h$  in Fig. 5 (indicated by tic marks) shifts linearly with photon energy, pointing toward a critical point in the final-state bands.<sup>25</sup> Indeed, we can

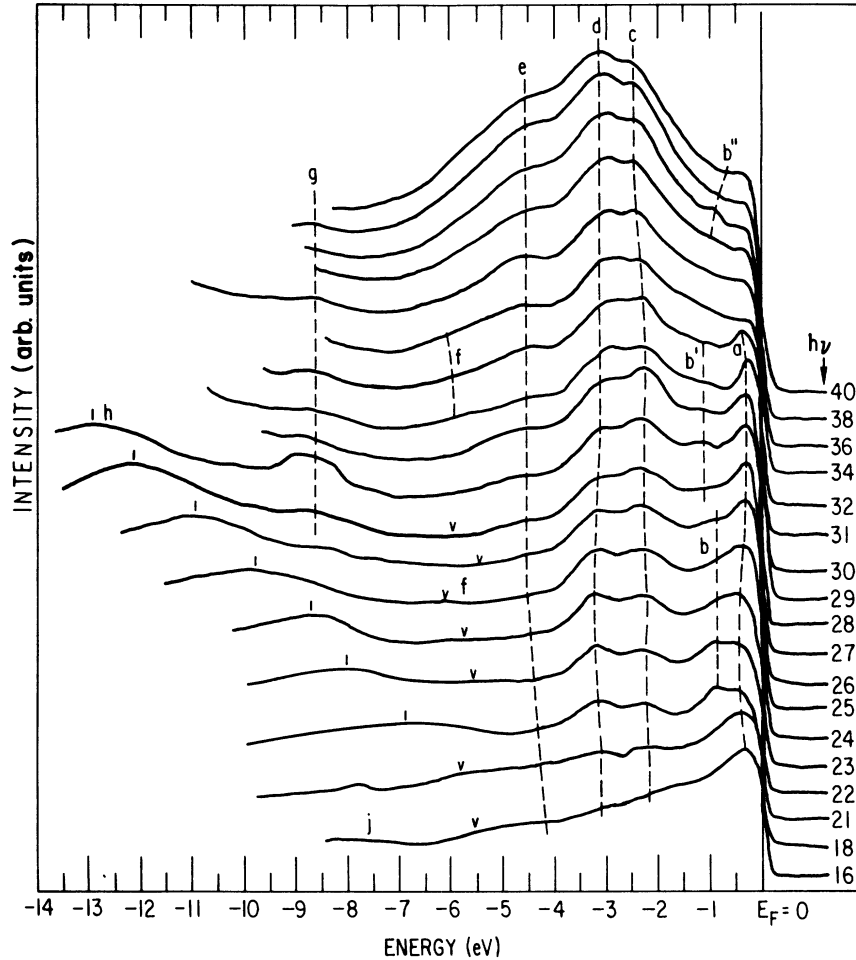


FIG. 5. Normal-emission EDC's for a UIr<sub>3</sub>(100) surface. Feature *g* is a surface impurity. Feature *h* (denoted by tick marks) is due to a final-state critical point at  $\sim 14$  eV.

use its final-state energy,  $E_f(\vec{k}_f) = 14.0$  eV, to construct a semiempirical final-state band along the  $\Gamma$ - $X$  line, which, in the simplest approximation, we assume is parabolic or free-electron-like ( $s$ - $p$ ), as in Ref. 24. Thus

$$E_f(\vec{k}) = 3.84 |\vec{k}_{\langle 100 \rangle} + \vec{G}_{\langle 100 \rangle}|^2 + \phi$$

with an experimentally determined work function of  $\phi = 5.0 \pm 0.3$  eV, and  $|\vec{G}_{\langle 100 \rangle}^{\Gamma X}| = \pi/a = 0.781 \text{ \AA}^{-1}$ . The best experimental fit was obtained for the case where  $k=0$  is located at  $X$  rather than at  $\Gamma$ , thus yielding the critical points at 5.0 and 14.37 eV at  $X$ , and at 7.34 and 26.08 eV at  $\Gamma$ . The 26.08-eV critical point explains the amplitude maximum observed for peak *a* at  $h\nu = 26$  eV. In a similar fashion peaks *b'* and *c* located at  $\sim -1$  and  $\sim -2$  eV have a maximum amplitude at  $h\nu = 27$  and 28 eV, respectively, consistent with this same critical point in the final state.

It is known<sup>26</sup> that normal-emission data can be

explained as being due to direct vertical transitions (i.e.,  $k_{\perp}$ -conserving) from initial states into this parabolic final state, and we use it to determine  $k_{\perp}$  for the occupied bands along  $\Gamma X$ . The experimental band structure thus derived is shown in Fig. 6, superimposed on the calculated bands. (The experimental points shown along  $\Gamma M$  are discussed below.) In general, the overall agreement is quite good particularly for the flat, high-density-of-states bands (resulting in the most prominent photoemission peaks *c* and *d*) at  $E_i \approx -2.3$  and  $-3.2$  eV. The hybridized  $f$ - $d$  bands (extending down to  $-2.5$  eV as derived from resonant photoemission of Fig. 3) are determined quite well at the zone center and boundary. We need not be concerned with the poor fit of points *e* since it is understood as discussed above, except insofar as the  $k$  broadening affects other data. Thus *b'* and *b''* are not included in the reduced data because of suspected  $k$  broadening.

In Fig. 7 we present angle-resolved EDC's for  $h\nu = 26$  eV and polar angles  $2^\circ < \theta < 15^\circ$  in the  $\langle 100 \rangle$

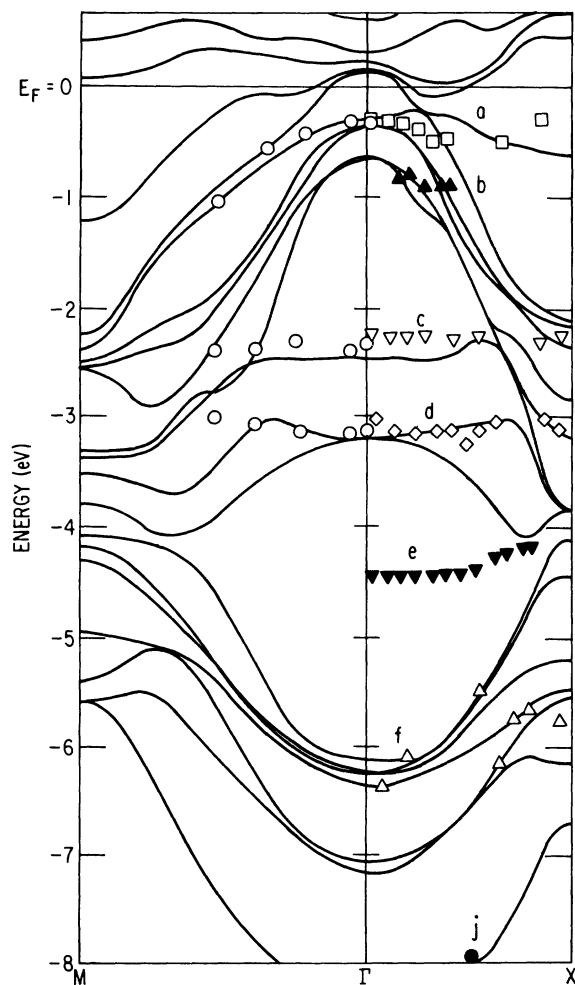


FIG. 6. Experimental data points superimposed on a theoretical band structure described in Sec. III. Data along the  $\Gamma$ - $X$  line are normal-emission data obtained by varying the photon energy. Data along the  $\Gamma$ - $M$  line were obtained at  $h\nu=26$  eV while varying the polar angle.

azimuth. In off-normal emission, assignment of the various peaks to interband bulk transitions is not trivial (e.g., Ref. 26). Direct transitions may take place over the entire plane bounded by  $\Gamma$ ,  $M$ , and  $X$ . In addition, Grandke *et al.*<sup>27</sup> point out that nonconservation of  $k_{\perp}$  is more likely to occur in off-normal directions, particularly in these high- $z$  materials which also have a small Brillouin zone. In this case peaks in the photocurrent may represent peaks in the one-dimensional density of states<sup>27</sup> which are most often obtained along high-symmetry lines. Whatever the situation, then, while we cannot be certain of the precise location of the observed transi-

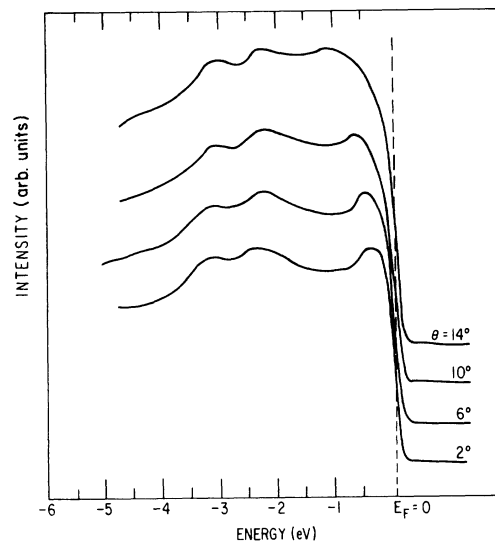


FIG. 7. EDC's obtained for a  $\text{UIr}_3(100)$  surface by varying the detector polar angle in the (001) plane at  $h\nu=26$  eV. Normal emission is at  $\theta=0^\circ$ .

tions, the excellent fit of the data with calculated bands along the  $\Gamma$ - $M$  line (see Fig. 6) is our principal justification in choosing this direction to compare to our data.

## V. CONCLUSIONS

It appears that resonant photoemission is a powerful tool in determining  $f$ -orbital character in photoemission features and extracting a partial  $f$  density of states in itinerant systems. The agreement with calculations in  $\text{UIr}_3$  is good. Dispersion has been observed for the first time in a photoemission peak which is clearly  $f$ -like in character. Good agreement is obtained with calculations for the flat, isolated  $d$  bands along  $\Gamma$ - $X$ , but rapid  $k$  broadening with  $h\nu$ , together with dense clustering of bands, prevents a more extensive observation of dispersion.

## ACKNOWLEDGMENTS

We thank G. Hollinger for his help in taking some of the data and the staff of the Synchrotron Radiation Center of the University of Wisconsin—Madison for the excellent support. The IBM 2D spectrometer is supported by the U. S. Air Force Office for Scientific Research under Contract No. F49620-81-C0089. The work at Argonne National Laboratory is supported by the U. S. Department of Energy.

- <sup>1</sup>See for example, *The Actinides: Electronic Structure and Related Properties*, edited by A. J. Freeman and J. B. Darby (Academic, New York, 1974).
- <sup>2</sup>B. Reihl, N. Mårtensson, D. E. Eastman, and O. Vogt, *Phys. Rev. B* **24**, 406 (1981).
- <sup>3</sup>B. Reihl, N. Mårtensson, P. Heimann, D. E. Eastman, and O. Vogt, *Phys. Rev. Lett.* **46**, 1480 (1981).
- <sup>4</sup>A. J. Freeman and D. D. Koelling, in *The Actinides: Electronic Structure and Related Properties*, edited by A. J. Freeman and J. B. Darby (Academic, New York, 1974), Vol. 1, pp. 51–108.
- <sup>5</sup>U. Fano, *Phys. Rev.* **124**, 1886 (1961).
- <sup>6</sup>R. Baptist, M. Belakhovsky, M. S. S. Brooks, R. Pinchaux, Y. Baer, and O. Vogt, *Physica (Utrecht) B* **102**, 63 (1980).
- <sup>7</sup>M. Iwan, E. E. Koch, and F.-J. Himpsel, *Phys. Rev. B* **24**, 613 (1981).
- <sup>8</sup>B. Reihl, N. Mårtensson, D. E. Eastman, A. J. Arko, and O. Vogt, *Phys. Rev. B* **26**, 1842 (1982).
- <sup>9</sup>J. W. Allen, S.-J. Oh, I. Lindau, J. M. Lawrence, L. I. Johansson, and S. B. Hagström, *Phys. Rev. Lett.* **46**, 1100 (1981).
- <sup>10</sup>A. J. Arko, M. B. Brodsky, G. W. Crabtree, D. Karim, D. D. Koelling, and L. R. Windmiller, *Phys. Rev. B* **12**, 4102 (1975).
- <sup>11</sup>D. D. Koelling and A. J. Freeman, in *Plutonium 1975 and Other Actinides*, edited by H. Blank and R. Linder (North-Holland, Amsterdam, 1976), p. 291.
- <sup>12</sup>A. J. Arko, M. B. Brodsky, G. W. Crabtree, and J. B. Ketterson, in Ref. 11, p. 325.
- <sup>13</sup>A. J. Arko, in *Proceedings of the Second International Conference on the Electronic Structure of the Actinides*, edited by J. Mulak, W. Suski, and R. Troć (Ossolineum, Wrocław, 1977), p. 309.
- <sup>14</sup>D. D. Koelling, in Ref. 13, p. 295.
- <sup>15</sup>T. W. Orent, S. D. Bader, and M. B. Brodsky, *Surf. Sci.* **75**, L385 (1978).
- <sup>16</sup>D. E. Eastman, J. J. Donelon, N. C. Hien, and F. J. Himpsel, *Nucl. Instrum. Methods* **172**, 327 (1980).
- <sup>17</sup>L. F. Mattheiss, *Phys. Rev.* **151**, 450 (1966); D. D. Koelling, *ibid.* **188**, 1049 (1969); D. D. Koelling, A. J. Freeman, and F. M. Mueller, *Phys. Rev. B* **1**, 1318 (1970).
- <sup>18</sup>A. J. Arko and D. D. Koelling, *Phys. Rev. B* **17**, 3104 (1978).
- <sup>19</sup>Y. Baer, H. R. Ott, and K. Andres, *Solid State Commun.* **36**, 387 (1980).
- <sup>20</sup>J. B. Pendry and J. F. L. Hopkinson, *J. Phys. F* **8**, 1009 (1978).
- <sup>21</sup>C. Kunz, in *Photoemission in Solids II*, edited by L. Ley and M. Cardona (Springer, Heidelberg, 1978), p. 315.
- <sup>22</sup>B. W. Veal, D. J. Lam, H. Diamond, and H. R. Hoekstra, *Phys. Rev. B* **15**, 2929 (1977).
- <sup>23</sup>P. J. Feibelman and D. E. Eastman, *Phys. Rev. B* **10**, 4932 (1974).
- <sup>24</sup>J. F. Van der Veen, F. J. Himpsel, and D. E. Eastman, *Solid State Commun.* **34**, 33 (1980).
- <sup>25</sup>F. J. Himpsel, *Appl. Opt.* **19**, 3964 (1980).
- <sup>26</sup>N. V. Smith, in *Photoemission in Solids I*, edited by M. Cardona and L. Ley (Springer, Heidelberg, 1978), p. 237.
- <sup>27</sup>T. Grandke, L. Ley, and M. Cardona, *Phys. Rev. B* **18**, 3847 (1978).